

**NON-CONVEX OPTIMIZATION METHODS
FOR ENHANCED PERFORMANCE FOR
PROBLEMS IN GRAPH SIGNAL
PROCESSING, PHASE-RETRIEVAL AND
SENSING**

GHANIA FATIMA



CENTRE FOR APPLIED RESEARCH IN ELECTRONICS

INDIAN INSTITUTE OF TECHNOLOGY DELHI

July 2025

© **Indian Institute of Technology Delhi (IITD), New Delhi, 2025**

**Non-convex Optimization Methods for Enhanced
Performance for Problems in Graph Signal
Processing, Phase-Retrieval and Sensing**

by

GHANIA FATIMA

CENTRE FOR APPLIED RESEARCH IN ELECTRONICS

Submitted

in fulfillment of the requirements of the degree of Doctor of Philosophy

to the



INDIAN INSTITUTE OF TECHNOLOGY DELHI

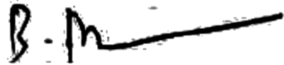
July 2025

*Dedicated to my Ammi and Abbu, and the unwavering
resilience of the people of Palestine.*

Certificate

This is to certify that the thesis entitled “**Non-convex Optimization Methods for Enhanced Performance for Problems in Graph Signal Processing, Phase-Retrieval and Sensing**”, submitted by **Ghania Fatima** to the Indian Institute of Technology Delhi, for the award of the degree of **Doctor of Philosophy** in Data Science and Signal Processing, is a record of the original, bona fide research work carried out by her under my supervision and guidance. The thesis has reached the standards fulfilling the requirements of the regulations related to the award of the degree.

The results contained in this thesis have not been submitted in part or in full to any other University or Institute for the award of any degree or diploma to the best of my knowledge.



Prof. Prabhu Babu

Thesis Supervisor

Centre for Applied Research in Electronics,
Indian Institute of Technology Delhi.

Acknowledgements

All praise is for **Allah**, the most merciful, who has granted me the strength, patience, and perseverance to complete this journey.

I express my deepest gratitude to *Prof. Prabhu Babu*, my PhD supervisor, whose mentorship, guidance, patience, and support have been invaluable throughout this journey. His dedication to research instilled in me a deeper appreciation for the field, inspiring me to pursue my work with sincerity and perseverance. He recognized when I struggled, offering encouragement and understanding, allowing me the space to find my way back. His belief in my potential, even when I doubted myself, has been one of the greatest gifts I received during this PhD. I am fortunate to have had a mentor who not only shaped my research but also reminded me of my own strength.

I also appreciate the contributions of my *Student Research Committe* (SRC) members, *Prof. Ananjan Basu*, *Prof. Monika Aggarwal*, and *Prof. Arpan Chattopadhyay*, whose insightful feedback significantly enriched this work.

I sincerely thank my collaborators *Prof. Petre Stoica*, *Prof. Antonio De Maio*, *Prof. Augusto Aubrey*, and *Prof. Aakash Arora* whose expertise and guidance contributed to my research. Working with esteemed professors in the field has been an honor and a learning experience.

I would also like to express my heartfelt gratitude to the C.A.R.E. office staff for their exceptional support and efficiency in managing administrative matters. A special thanks to *Sameer Hansda*, who was not just a great support but also a wonderful friend throughout this journey.

Pursuing a Ph.D. is a journey filled with challenges, and I have been fortunate to have incredible friends along this path who made the experience lighter and more meaningful. I thank *Soham Das*, *Anchita Dey*, *Venkatesh Pillai*, *Shweta Yadav*, and *Shweta Pal* who have been with me since my course-work and whose companionship has been invaluable. I would also like to acknowledge my labmates, *Kuntal Panwar*, *Prasanth Logaraman*, *Piyush Varshney*, *Astha Saini*, *Surabhi Soni*, *Pushpendra Rajpurohit*, *Mintu Kumar*, *Ankush Koundal*, *Basharat Rashid*, *Shahnoor Ali* and *Sourav Banerjee* for their camaraderie, discussions, and support. A very special

mention to *Toiba Noor*, *Syed Afzal Hashmi*, and *Jasleen Kaur* for being my pillars of support. Their encouragement, understanding, and belief in me have meant the world, and I could not have asked for better friends to lean on. Beyond the lab, I am grateful to *Mohd Imran Khan*, *Waris Khan*, *Tehreem Zaidi*, and *Kritika Tandon* for their friendship and unwavering presence at all times, sharing moments of joy and frustration. My childhood friends, *Kirti Manjusha*, *Richa Ruchikar*, *Sadaf Noori*, *Arfa Jabin*, *Nida Tahreem*, *Safa Tanzeem* and *Ilma Ansar* have been my constants, offering their love and encouragement even from afar. Their presence in my life reminds me of where I come from and the roots that keep me grounded. My heartfelt appreciation goes to my cousins *Fahad Imam*, *Shaghaf Manawar*, and *Alfa Fatima*, who have been my family away from home. Your warmth and support have made the toughest days more bearable, and I am forever grateful for the love you have extended to me.

I owe everything to my family, whose unwavering love and support have been my greatest strength. My father, *Syed Ozair Ahmad*, took immense pride in every achievement of mine, big or small, and his belief in me kept me motivated through every challenge. My mother, *Razia Shaheen*, a passionate advocate for women's education, has been my pillar of strength, without whom I would have crumbled. My sisters, *Altaf Ozair* and *Fareya Ozair*, have been my guiding lights, constantly inspiring me to reach greater heights. My brothers, *Nashit Ozair* and *Ahzam Ozair*, fill my life with enjoyment and fun. My brothers-in-law, *Meraj Nawaz* and *Nadeem Anwar*, are more like brothers, always offering warmth and support. And finally, my dearest nephew, *Hammad*, who turns five as I submit this thesis, has been a source of endless love and serenity. His presence has made this five-year PhD journey lighter, filling it with cherished moments of joy and comfort.

Thank you all.

Ghania Fatima
Ghania Fatima

Abstract

The complexity of optimization problems varies based on the nature of the objective function, constraints, and structural properties such as sparsity and rank deficiency. While convex optimization offers well-established solution techniques with strong theoretical guarantees, many real-world problems are inherently non-convex solving which remains a significant challenge, making non-convex optimization an active area of research in science and engineering. This thesis aims to develop efficient algorithms for solving non-convex problems across three research areas: graph signal processing, phase-retrieval, and sensing, primarily leveraging and extending classical methods like block coordinate descent (BCD) and majorization-minimization (MM).

In the area of **graph signal processing**, this thesis first proposes an MM-based algorithm to learn a sparse weighted graph by estimating its adjacency matrix under the assumption that observed signals vary smoothly over the graph nodes. Notably, the proposed algorithm requires no hyperparameter tuning and features automatic elimination of inactive variables during iterations, enhancing computational efficiency. Next, the thesis addresses the challenge of learning graphs in the presence of outliers by maximizing the penalized log-likelihood of the uncorrupted data, selecting the penalty using the false discovery rate (FDR) principle, while simultaneously estimating the number and locations of outliers and the precision matrix under graph Laplacian constraints. The thesis also considers covariance matrix estimation under positivity and sparsity constraints. It first introduces a BCD-based maximum likelihood estimation method for estimating covariance matrices with non-negative off-diagonal elements, which has applications to portfolio selection in finance. Next, a two-stage procedure is proposed for estimating sparse covariance matrices. First, the sparsity pattern of the target covariance matrix is estimated using an FDR-based multiple-hypothesis testing method. Then, the nonzero values are estimated using either a BCD or a proximal distance approach. Lastly, the thesis presents a unified framework for estimating sparse covariance matrices by integrating sparsity pattern selection and covariance matrix estimation in a single step, eliminating the need for hyperparameter tuning. A cyclic majorization-minimization technique is introduced within this framework to solve an ℓ_0 -norm penalized MLE problem.

Under **phase-retrieval**, the thesis first introduces a double-loop MM algorithm to recover the original signal from measurements that contain only the magnitude of a linear function of the unknown signal, where the measurement noise follows a Poisson distribution. This is achieved by reformulating the original minimization problem into a saddle-point problem. The thesis further extends the algorithm to handle various ℓ_1 regularized Poisson phase-retrieval problems (which exploit sparsity). Additionally, the thesis proposes an iterative algorithm for the phase-retrieval problem under the scenario when the measurements follow Poisson plus Gaussian (PG) distribution, which is a more realistic model in applications like astronomy, microscopy, medical imaging, and remote sensing. The proposed algorithms are compared with previously proposed algorithms under different experimental settings.

In the area of **sensing**, the thesis undertakes the problems of optimal placement of sensors for improving the accuracy of various source localization techniques. First, the thesis presents an optimal sensor placement methodology, based on MM, for the hybrid localization technique by reformulating the problem into a saddle-point problem. The proposed method is designed for A -, D -, and E - optimality criteria and can work for both uncorrelated and correlated noise in the measurements. Next, the thesis proposes a numerical method for the optimal placement of the receivers in a multistatic target localization system (with a single transmitter and multiple receivers) using A - and D - optimality criteria. The proposed algorithm, based on the principle of block majorization minimization (block MM), can also handle the cases where the transmitter also acts as a receiver. Lastly, the thesis focuses on finding the optimal sensor placements for source localization without any specific assumption on the actual source position and considering just a region where the source is likely to be present, yielding a robust design. Moreover, each sensor position is constrained to lie within a pre-specified set (deployment constraint set). The proposed methodology, based on Block-MM, can also handle the case of nonuniform noise variances.

The numerical simulation analysis of all the methods proposed in the thesis over both synthetic and real-world data demonstrates their superior performance over the state-of-the-art algorithms.

सार

अनुकूलन समस्याओं की जटिलता उद्देश्य फ्रंक्शन, बाधाओं और संरचनात्मक गुणों जैसे कि विरलता और रैंक की कमी की प्रकृति के अनुसार बदलती रहती है। जबकि उत्तल अनुकूलन अच्छी तरह से स्थापित समाधान तकनीकों और मजबूत सैद्धांतिक गारंटियों को प्रदान करता है, कई वास्तविक दुनिया की समस्याएं स्वाभाविक रूप से गैर-उत्तल होती हैं, जिनका समाधान एक महत्वपूर्ण चुनौती बना रहता है। यही कारण है कि गैर-उत्तल अनुकूलन विज्ञान और अभियांत्रिकी में शोध का एक सक्रिय क्षेत्र बना हुआ है। यह शोध प्रबंध तीन शोध क्षेत्रों—ग्राफ सिग्नल प्रोसेसिंग, चरण-पुनर्प्राप्ति और संवेदन में गैर-उत्तल समस्याओं के समाधान के लिए कुशल एल्गोरिदम विकसित करने का उद्देश्य रखता है, जो मुख्य रूप से ब्लॉक कोऑर्डिनेट डीसेंट (बीसीडी) और मेजराइज़ेशन-मिनिमाइज़ेशन (एमएम) जैसी पारंपरिक विधियों का उपयोग और विस्तार करता है।

ग्राफ सिग्नल प्रोसेसिंग के क्षेत्र में, यह शोध पहले एक एमएम आधारित एल्गोरिदम प्रस्तावित करता है, जो एक विरल भारित ग्राफ को सीखने के लिए उसके सिग्नल कटता मैट्रिक्स का अनुमान लगाता है, इस धारणा के तहत कि प्रेक्षित सिग्नल ग्राफ नोड्स पर सहज रूप से परिवर्तित होते हैं। विशेष रूप से, इस प्रस्तावित एल्गोरिदम को किसी हाइपरपैरामीटर ट्यूनिंग की आवश्यकता नहीं होती है और यह पुनरावृत्तियों के दौरान निष्क्रिय चरण को स्वचालित रूप से हटा देता है, जिससे गणना दक्षता में वृद्धि होती है। अगले चरण में, यह शोध प्रबंध बाह्य मानों की उपस्थिति में ग्राफ सीखने की चुनौती को संबोधित करता है। यह बिना विकृत डेटा के दंडित लॉग-लाइकलीहुड को अधिकतम करके ग्राफ सीखने का प्रयास करता है, जहाँ दंड का चयन गलत खोज दर (एफडीआर) सिद्धांत के आधार पर किया जाता है। साथ ही, यह बाह्य मानों की संख्या और स्थानों का अनुमान लगाने के साथ-साथ ग्राफ लैप्लासियन बाधाओं के तहत परिशुद्धता मैट्रिक्स का भी अनुमान लगाता है। यह शोध प्रबंध सकारात्मकता और विरलता बाधाओं के तहत सहप्रसरण मैट्रिक्स के अनुमान पर भी विचार करता है। सबसे पहले, यह एक बीसीडी आधारित अधिकतम संभावना अनुमान (एमएलई) विधि प्रस्तुत करता है, जो गैर-नकारात्मक ऑफ-डायगोनल तत्वों वाले सहसंबंध मैट्रिक्स का अनुमान लगाने के लिए उपयोग की जाती है। इसका विचार में पोर्टफोलियो चयन जैसे अनुप्रयोगों में उपयोग किया जा सकता है, विरल सहप्रसरण मैट्रिक्स के अनुमान के लिए एक द्वि-चरणीय प्रक्रिया प्रस्तावित की गई है। सबसे पहले, लक्ष्य सहप्रसरण मैट्रिक्स की विरलता पैटर्न को एफडीआर-आधारित बहु-परिकल्पना परीक्षण विधि का उपयोग करके अनुमानित किया जाता है। इसके बाद, गैर-शून्य मानों का अनुमान या तो बीसीडी या प्रोक्सिमल डिस्टेंस दृष्टिकोण का उपयोग करके लगाया जाता है, जो अनुमानित सहप्रसरण ग्राफ से विचलनों को दंडित करता है। अंततः, यह शोध प्रबंध विस्तारित बेयेज़ सूचना मानदंड (ईबीआईसी), जो एक उच्च-आयामी मॉडल चयन नियम है, का उपयोग करके ℓ_0 -नॉर्म दंडित एमएलई समस्या को हल करके विरल सहसंबंध मैट्रिक्स के अनुमान के लिए एक एकीकृत रूपरेखा प्रस्तुत करता है। यह दृष्टिकोण विरलता पैटर्न चयन और सहसंबंध मैट्रिक्स के अनुमान को एक ही चरण में एकीकृत करता है, जिससे हाइपरपैरामीटर ट्यूनिंग की आवश्यकता समाप्त हो जाती है। इस रूपरेखा के अंतर्गत एक चक्रीय एमएम तकनीक प्रस्तुत की गई है।

चरण-पुनर्प्राप्ति के तहत, यह शोध प्रबंध पहले एक द्वि-चक्र एमएम एल्गोरिदम प्रस्तुत करता है, जो केवल अज्ञात सिग्नल के एक रैखिक फलन के परिमाण वाली मापों से मूल सिग्नल को पुनर्प्राप्त करने के लिए डिज़ाइन किया गया है। यहाँ मापित शोर पॉइसॉन वितरण का अनुसरण करता है। यह मूल लघुकरण समस्या को एक सैडल-पॉइंट समस्या में पुनःसंरचित करके प्राप्त किया जाता है। यह शोध प्रबंध आगे इस एल्गोरिदम का विस्तार विभिन्न ℓ_1 -नियमितकृत पॉइसॉन चरण-पुनर्प्राप्ति समस्याओं (जो विरलता का लाभ उठाती हैं) को संभालने के लिए करता है। इसके अतिरिक्त, शोध प्रबंध उस परिदृश्य के तहत चरण-पुनर्प्राप्ति समस्या के लिए एक पुनरावृत्त एल्गोरिदम का प्रस्ताव करता है, जब मापित पॉइसॉन-प्लस-गॉसियन (पीजी) वितरण का पालन करते हैं, जो खगोल विज्ञान, सूक्ष्मदर्शी, चिकित्सा इमेजिंग और रिमोट सेंसिंग जैसे अनुप्रयोगों में एक अधिक यथार्थवादी मॉडल है। प्रस्तावित एल्गोरिदम की तुलना पहले से प्रस्तावित एल्गोरिदम से विभिन्न प्रयोगात्मक परिस्थितियों में किया गया है।

संवेदन के क्षेत्र में, यह शोध प्रबंध विभिन्न स्रोत स्थानीयकरण तकनीकों की सटीकता में सुधार के लिए सेंसरों की इष्टतम स्थिति निर्धारण की समस्याओं को संबोधित करता है। सबसे पहले, यह शोध प्रबंध संकर स्थानीयकरण तकनीक के लिए एमएम आधारित इष्टतम सेंसर स्थान निर्धारण विधि प्रस्तुत करता है, जिसमें समस्या को सैडल-पॉइंट समस्या के रूप में पुनः स्वरूपित किया जाता है। प्रस्तावित विधि को A-, D- और E- इष्टतमता मानदंडों के लिए डिज़ाइन किया गया है और यह माप में असंबद्ध तथा सहसंबद्ध शोर दोनों के साथ कार्य कर सकती है। इसके बाद, शोध प्रबंध एक संख्यात्मक विधि प्रस्तुत करता है, जो A- और D- इष्टतमता मानदंडों का उपयोग करके एक बहुस्तरीय लक्ष्य स्थानीयकरण प्रणाली (जिसमें एक ट्रांसमीटर और कई रिसेवर्स होते हैं) में रिसेवर्स की इष्टतम स्थिति निर्धारित करने के लिए बनाई गई है। ब्लॉक एमएम के सिद्धांत पर आधारित प्रस्तावित एल्गोरिदम उन मामलों को भी संभाल सकता है जहां ट्रांसमीटर स्वयं रिसेवर के रूप में कार्य करता है। अंततः, यह शोध प्रबंध स्रोत स्थानीयकरण के लिए सेंसर के इष्टतम स्थान चयन पर केंद्रित है, बिना किसी विशिष्ट धारणा के कि स्रोत वास्तव में कहाँ स्थित है। इसके बजाय, केवल उस क्षेत्र को ध्यान में रखा गया है जहाँ उसके मौजूद होने की संभावना अधिक है, जिससे एक मजबूत और प्रभावी डिज़ाइन प्राप्त होता है। इसके अलावा, प्रत्येक सेंसर की स्थिति को एक पूर्व-निर्धारित सेट (तैनाती बाधा सेट) के भीतर रहने की बाध्यता होती है। प्रस्तावित विधि, जो ब्लॉक-एमएम पर आधारित है, असमान शोर प्ररूपों के मामलों को भी संभाल सकती है।

प्रस्तावित सभी विधियों का संख्यात्मक सिमुलेशन विश्लेषण, सिंथेटिक और वास्तविक डेटा दोनों पर, उन्हें आधुनिकतम एल्गोरिदम की तुलना में श्रेष्ठ प्रदर्शन दर्शाता है।

Contents

Certificate	i
Acknowledgements	iii
Abstract	v
Contents	ix
List of Figures	xv
List of Tables	xxiii
Abbreviations	xxv
Notations	xxvii
1 Introduction	1
1.1 Types of Optimization problems	2
1.1.1 Solving Optimization Problems	5
1.2 Applications	6
1.2.1 Graph signal processing	7
1.2.1.1 Motivation	8
1.2.1.2 Key contributions	9
1.2.2 Phase-retrieval	10
1.2.2.1 Motivation	11
1.2.2.2 Key Contributions	11
1.2.3 Sensing	12
1.2.3.1 Motivation	15
1.2.3.2 Key contributions	15
1.3 Thesis organization	16

2	Optimization Techniques	23
2.1	Block Coordinate Descent	23
2.2	Majorization Minimization	24
2.3	Block Majorization-Minimization	26
2.4	Primal-Dual Majorization-Minimization	27
2.5	Proximal Distance	28
3	Graph Signal Processing	31
3.1	Learning sparse graphs for smooth node signals	33
3.1.1	Literature Review and Problem Formulation	33
3.1.2	Proposed Method	35
3.1.2.1	Computational Complexity and Convergence	38
3.1.3	Simulation Results	39
3.1.3.1	Synthetic graph	39
3.1.3.2	Brain network	41
3.1.4	Conclusion	43
3.2	Graph Learning in the Presence of Outliers	44
3.2.1	Literature review and Problem Formulation	44
3.2.1.1	Graphical Gaussian model	44
3.2.1.2	Graph Data with Outliers	47
3.2.1.3	Problem Formulation	49
3.2.2	Proposed Method	51
3.2.2.1	Computational Complexity and Convergence	62
3.2.3	Simulation Results	62
3.2.3.1	Convergence	64
3.2.3.2	Visualization of outlier detection	64
3.2.3.3	Graph learning for Synthetic data	66
3.2.3.4	Graph Learning for Real data	70
3.2.4	Conclusion	74
3.3	Covariance matrix estimation under positivity constraints	74
3.3.1	Literature Review and Problem Formulation	74
3.3.2	Proposed Algorithm	77
3.3.2.1	Majorization-minimization based approach	77
3.3.2.2	Block Coordinate Descent based approach	78
3.3.2.3	Computational Complexity	82
3.3.3	Numerical Simulation results	84
3.3.3.1	Synthetic data	84
3.3.3.2	Real-world financial data	86
3.3.4	Conclusion	87
3.4	Covariance matrix estimation under sparsity constraints	88
3.4.1	Literature Review and Problem Formulation	88
3.4.1.1	Graph Motivation	90

3.4.1.2	Literature review	90
3.4.1.3	Contributions	93
3.4.2	Proposed Methodology	95
3.4.2.1	First Stage: Hypothesis testing	95
3.4.2.2	Second Stage: Solving the MLE through Block Co- ordinate Descent method	98
3.4.3	Numerical Simulations	109
3.4.4	Synthetic data	109
3.4.5	Real data	115
3.4.5.1	Migration data	117
3.4.5.2	Cell signalling data	118
3.4.6	Conclusions	120
3.5	Covariance matrix estimation under sparsity constraints: Hyper-parameter- tuning-free algorithm	121
3.5.1	Literature Review and Problem Formulation	121
3.5.2	Proposed Methodology	122
3.5.2.1	Sparse Covariance Estimation Framework	122
3.5.2.2	Cyclop	123
3.5.3	Numerical Simulations	129
3.5.4	Conclusions	131
4	Phase-Retrieval	133
4.1	Phase-retrieval for Poisson data model	137
4.1.1	Introduction and Literature review	137
4.1.1.1	Contributions	138
4.1.2	Problem formulation and Proposed method	140
4.1.2.1	PDMM for regularized Poisson phase-retrieval problem	150
4.1.2.2	Computational Complexity of PDMM	155
4.1.2.3	Convergence Analysis of PDMM	156
4.1.3	Numerical Simulations	159
4.1.3.1	Initialization and convergence threshold	160
4.1.3.2	Ambiguities and Performance Evaluation	161
4.1.3.3	Experimental Settings	162
4.1.3.4	Simulation Results	164
4.1.4	Conclusions	170
4.2	Phase-retrieval for Poisson plus Gaussian data model	171
4.2.1	Problem Formulation	172
4.2.2	Proposed Method	173
4.2.2.1	Computational complexity and Convergence analysis	178
4.2.3	Numerical results	178
4.2.4	Conclusions	182

5 Sensing	183
5.1 Optimal Sensor Placement for Hybrid Source Localization	188
5.1.1 Introduction and Literature review	188
5.1.1.1 Contributions	190
5.1.2 Problem Formulation	192
5.1.3 Proposed Method	199
5.1.3.1 Proposed method for A -optimal design	199
5.1.3.2 Proposed algorithm for D - and E -optimal design	206
5.1.3.3 Computational complexity and proof of convergence	211
5.1.4 Numerical simulation results	213
5.1.4.1 Convergence of the proposed algorithm	213
5.1.4.2 Proposed algorithm for the 3D case	215
5.1.4.3 Performance in the presence of uncorrelated noise measurements	216
5.1.4.3.1 Optimal design for uniform sensor-target ranges	217
5.1.4.3.2 Optimal design for nonuniform sensor-target range	219
5.1.4.4 Mean Square Error (MSE) analysis	221
5.1.4.5 Performance analysis of the proposed method for mismatch in the target location estimate	221
5.1.5 Conclusions	224
5.2 Optimal Receivers Placement for Multistatic Source Localization	224
5.2.1 Introduction and literature review	225
5.2.1.1 Contributions	228
5.2.2 Problem Formulation	229
5.2.3 Proposed MM method	233
5.2.3.1 Proposed algorithm for A -optimal design	236
5.2.3.2 Computational complexity and convergence	239
5.2.4 Numerical simulation	239
5.2.4.1 Optimal placement of receivers	241
5.2.4.2 The transmitter is also a receiver	249
5.2.4.3 MSE analysis	254
5.2.5 Conclusions	256
5.3 Robust Sensor Placement for TOA or RSS Source localization	257
5.3.1 Introduction and literature review	258
5.3.1.1 Contributions	260
5.3.2 Problem Formulation	260
5.3.2.1 TOA Source Localization Model	260
5.3.2.2 RSS Source Localization Model	266
5.3.3 Proposed Method	268
5.3.3.1 Sensor Placements Problem for TOA Based Local- ization	268

5.3.3.2	Sensor Placements Problem for RSS Based Localization	274
5.3.3.3	Computational Complexity and Convergence of the Proposed Method	277
5.3.4	Numerical Results	280
5.3.4.1	Sensor Placements in 2D Scenarios	281
5.3.4.2	Sensor Placements in 3D Scenarios	287
5.3.4.3	MSE comparison	290
5.4	Conclusion	292
6	Conclusion and Scope of Future work	293
6.1	Conclusion	293
6.2	Scope of future work	295
	References	297
A	Proof of convexity of the the first term in 3.35 in Section 3.2	347
B	Proof of concavity of the the second term in 3.35 in Section 3.2	349
C	CYCLOP_BCD: A block coordinate approach for the problem in Section 3.5	351
D	Lemma for Section 5.1	357
E	Detailed proofs of Lemma 5.7 and 5.8	359
E.1	Proof of Lemma 5.7	359
E.2	Proof of Lemma 5.8	361
F	Proof of the convexity of the function in (5.102) in Section 5.2.	363
G	Proof of Proposition in Section 5.3	365
	List of Publications	371
	Technical Biography of Author	375

List of Figures

1.1	An example of (a) a convex function with one global minimum; and (b) a non-convex function having one global minimum along with two local minima.	4
3.1	The objective function $f(\mathbf{w})$ and the surrogate function $g(\mathbf{w} \mathbf{w}^k)$ at $\mathbf{w}^k = [0.2 \ 0.2 \ 0.2]^T$. (a) $f(w_1, w_2 w_3 = 0.2)$ and $g(w_1, w_2 w_3 = 0.2 \mathbf{w}^k)$ vs w_1 and w_2 . (b) $f(w_1 w_2 = 0.2, w_3 = 0.2)$ and $g(w_1 w_2 = 0.2, w_3 = 0.2 \mathbf{w}^k)$ vs w_1	37
3.2	$f(\mathbf{w})$ vs iteration number for (a) ER graph (200 nodes) for $\alpha = 0.1$ and $\beta = 0.1$ and (b) SBM graph (300 nodes) for $\alpha = 0.1$ and $\beta = 0.1$	41
3.3	Visualization of adjacency matrices for (a) true ER graph for $p = 30$ nodes and (b) Estimated ER graph for $p = 30$ nodes.	41
3.4	$f(\mathbf{w})$ vs iteration number for (a) Brain graph with 66 ROIs for Subject 3 for $\alpha = 0.6310$ and $\beta = 0.1$, and (b) Brain graph with 66 ROIs for Subject 5 for $\alpha = 0.3981$ and $\beta = 0.1$	42
3.5	Objective function versus iteration for 30 random initializations when $p = 15$, $n = 50$ and $\beta = 0.1$	64
3.6	True positions (left) and positions estimated by Robgraph (right) of node outliers for $p = 15$, $n = 150$ and (a) $\beta = 0.01$ yielding outliers false alarms = 0 and outliers misses = 0, (b) $\beta = 0.1$ yielding outliers false alarms = 1 and outliers misses = 0 and (c) $\beta = 0.5$ yielding outliers false alarms = 7 and outliers misses = 0.	65
3.7	Variation of (a) P_{fa} , (b) P_{miss} and (c) MCC with β for $p = 30$ and $n = 300$ (top) and with n for $p = 30$ and $\beta = 0.1$ (bottom).	67
3.8	Ground Truth ER graph with $p = 15$ nodes.	68
3.9	(a) Graph estimated using the method in [1] ($P_{fa} = 0.26$; $P_{miss} = 0.075$); (b) graph estimated using the method in [2] ($P_{fa} = 0.09$; $P_{miss} = 0.01$); (c) Robgraph ($P_{fa} = 0$; $P_{miss} = 0$) when $\beta = 0.01$	69
3.10	Left: Graph estimated using the method in [1] ($P_{fa} = 0.36$; $P_{miss} = 0.11$); Middle: graph estimated using the method in [2] ($P_{fa} = 0.29$; $P_{miss} = 0.10$); and Right: Robgraph ($P_{fa} = 0.09$; $P_{miss} = 0.02$) when $\beta = 0.05$	69

3.11	(a) Ground truth ER graph with $p = 500$ nodes and (b) Robgraph when $n = 600$, the outlier percentage in the data is $\beta = 0.05$. The black dotted lines are misses and the red lines are false alarms.	70
3.12	<i>MRI data</i> : The graphs learned from uncorrupted data (a); and corrupted data using [1] (b), [2] (c) and Robgraph (d). The black dotted lines are misses and red solid lines are false alarms with the graph at the top-left as reference.	71
3.13	<i>Migration data</i> : Heatmaps of the estimated precision matrices when the graph is learned from uncorrupted data (top left); and from corrupted data using [1] (top right), [2] (bottom left) and Robgraph (bottom right).	72
3.14	<i>Ionosphere data</i> : The graphs learned from uncorrupted data (top left); and corrupted data using [1] (top right), [2] (bottom left) and Robgraph (bottom right). The black dotted lines are misses and red solid lines are false alarms with the graph at the top-left as reference.	73
3.15	(Left) $f(\mathbf{R})$ vs iteration for a data matrix $\mathbf{X} \in \mathbb{R}^{5 \times 10}$ using 30 random initializations. (Right) $f(\mathbf{R})$ vs time (s) for CODE and MM for another data matrix $\mathbf{X} \in \mathbb{R}^{5 \times 10}$	85
3.16	Synthetic data example: NRMSE of the estimated covariance matrix vs number of samples (N) for $P = 100$	86
3.17	Financial data example: Median value of the standard deviation obtained for every month from 84 out-of-sample data.	87
3.18	An example of a sparse covariance matrix with $p = 4$ variables and its associated graph.	91
3.19	(a) Variation of the sparsity obtained with FDR for different values of α and (b) Variation of EBIC for the selected values of α ($p = 30$, $n = 40$ and 80% sparsity).	111
3.20	Variation of the objective function with (a) Iteration index and (b) Time (seconds) for $p = 100$ and $n = 150$	111
3.21	(a) Objective function vs iteration for $p = 100$, $n = 150$ and sparsity = 75%; (b) Average time (s) needed by BCD and PD to converge for $n = 2p$ and 75% sparsity.	113
3.22	NRMSE vs sparsity for $p = 30$. The dashed curves show the NRMSE obtained with the sparsity pattern inferred via FDR and the solid curves show the NRMSE obtained with the true sparsity pattern.	114
3.23	Variation of NRMSE with number of samples (n) for (a) $p = 100$ and sparsity = 60% and (b) $p = 150$ and sparsity = 70%.	114
3.24	MCC vs the number of samples (n) for (a) $p = 100$ and (b) $p = 200$ with sparsity = 80% and n varying between 100 and 9000.	115

3.25	Two examples of estimated correlations of five countries. Example 1 (left-hand side): (a) Pearson correlation estimates; (c) EBIC vs α ; (e) Estimated correlations using BCD ($\alpha = 0.002$). Example 2 (right-hand side): (b) Pearson correlation estimates; (d) EBIC vs α ; (f) Estimated correlations using BCD ($\alpha = 0.065$)	116
3.26	(a)-(c) Estimated covariance graphs obtained using BCD; (d)-(f) Markov graphs obtained using the Graphical Lasso for precision matrix estimation; (g)-(i) Estimated covariance graphs obtained using the method of [3]; (j)-(l) Estimated covariance graphs obtained using the method of [4]. First column: $k = 16$ edges, second column: $k = 9$ edges and third column: $k = 6$ edges.	119
3.27	Estimated covariance graph using BCD with the value of α (0.004) obtained via EBIC.	120
3.28	Objective function versus iteration for $p = 50$ and $n = 150$ when the true covariance matrix has 75% sparsity.	129
3.29	Variation of (a) NRMSE and (b) KL divergence when $p = 100$, n varies between 60 and 140 and \mathbf{R}_{true} has a sparsity of 80%.	130
3.30	Average run time (s) vs p when $n = p$, p varies between 50 and 100 and \mathbf{R}_{true} has a sparsity of 80%.	130
4.1	A representative plot of majorizers for PDMM (satisfying the constraint in (4.26)) and MM [5] with $x_t = 4$ for the non-convex Poisson log-likelihood function.	145
4.2	Average computation time (in seconds) vs Number of measurements N , when $\eta = 10^{-6}$, $\mathbf{x} \in \mathbb{C}^{100}$ and \mathbf{A} is a random matrix. Sub-Figures (a) and (b) correspond to cases when $b_i = 0.1$ and $b_i = 0$ respectively.	165
4.3	NRMSE vs Number of measurements (N) for $\eta = 10^{-6}$, $\mathbf{x} \in \mathbb{C}^{100}$ and \mathbf{A} is a random matrix. Sub-Figure (a) and (b) correspond to the cases when $b_i = 0.1$ and $b_i = 0$ respectively.	165
4.4	Average computation time (in seconds) vs Length of original signal K , when $\eta = 10^{-6}$, $N = 4000$ and \mathbf{A} is a random matrix. Sub-Figures (a) and (b) corresponds to cases when $b_i = 0.1$ and $b_i = 0$, respectively.	166
4.5	NRMSE vs Length of original signal (K) for $\eta = 10^{-6}$, $N = 4000$ and \mathbf{A} being a random matrix. Sub-Figure (a) and (b) corresponds to the cases when $b_i = 0.1$ and $b_i = 0$, respectively.	167
4.6	NRMSE vs time when $N = 4000$, $\mathbf{x} \in \mathbb{C}^{300}$, $\eta = 10^{-6}$ and \mathbf{A} is a random matrix for unregularized phase-retrieval problem. Sub-Figure (a) and (b) correspond to the cases when $b_i = 0.1$ and $b_i = 0$, respectively.	167
4.7	NRMSE vs λ_{noise} when $N = 4000$, $\mathbf{x} \in \mathbb{C}^{300}$, $\eta = 10^{-6}$, $b_i = 0.1$, and \mathbf{A} is a random matrix.	168

4.8	(a) NRMSE vs Time when $N = 4000$ and $\mathbf{x} \in \mathbb{C}^{300}$. (b) NRMSE vs N when $K = 100$. (c) NRMSE vs K when $N = 4000$. The results are for ℓ_1 regularized phase-retrieval problem when \mathbf{A} is a random matrix and $b_i = 0.1$	169
4.9	Reconstructed images and corresponding NRMSE compared to the true image (Cameraman of size 128×128), for a measurement system with $M = 21$ masked DFT matrices and TV regularized phase-retrieval problem. (a) True Image; (b) PDMM (6.3%); (c) ADMM (6.9%); (d) MM (7.5%)	170
4.10	NRMSE vs time plot for a 128×128 Cameraman image for a measurement system with $M = 21$ masked DFT matrices and TV regularized phase-retrieval problem.	170
4.11	A representative figure showing the plots for the surrogate function using the three approximations of $\{\gamma_i(\mathbf{x}_t)\}$ and the original objective function for a one-dimensional example.	179
4.12	(a) NRMSE vs Iteration. (b) Objective function vs Iteration. The choice of parameters (wherever applicable) in different plots are $\sigma = 1.5$, $N = 5000$ and $K = 50$	179
4.13	(a) NRMSE vs Number of measurements (N). (b) Average time vs Number of measurements (N).	180
4.14	(a) NRMSE vs Length of original signal (K). (b) Average time vs Length of original signal (K).	180
4.15	NRMSE vs Standard deviation (σ).	180
5.1	Measurement geometry of the hybrid localization model. The blue triangle represents the target and the black circles are the sensors. p_1, p_2, p_3 and p_4 represent the RSS measurements, $\theta_1, \theta_2, \theta_3$ and θ_4 represent the AOA measurements, and ct_1, ct_2, ct_3 and ct_4 are the measurements corresponding to TOA.	192
5.2	Convergence plot and corresponding sensor placement for 2D hybrid TOA-RSS-AOA under correlated noise. Top: convergence plots; Bottom: sensor placement with black square: target; blue circle: initial sensors' positions; blue pentagram: final sensors' positions. (a) A -optimal design (for $r = 500$ meters); (b) D -optimal design (for $r = 100$ meters); (c) E -optimal design (for $r = 10$ meters)	214
5.3	Convergence plot and corresponding sensor placement for 3D hybrid TOA-RSS under correlated noise. Top: convergence plots; Bottom: sensor placement with black square: target; blue circle: initial sensors' positions; blue pentagram: final sensors' positions. (a) A -optimal design (for $r = 10$ meters); (b) D -optimal design (for $r = 10$ meters); (c) E -optimal design (for $r = 1$ meter)	215
5.4	Optimal sensor trajectories of (a) example 1 and (b) example 2, \circ : sensor initial position, $*$: sensor final position, \square : target position	218

5.5	Optimal sensor trajectories and the final geometries with different sensor initial positions for $m = 2$ and uniform d_i considered in subsection 5.1.4.3.1	219
5.6	Optimal sensor trajectories and the final geometries with different sensor start positions for $m = 3$ and uniform d_i considered in subsection 5.1.4.3.1.	219
5.7	Optimal sensor trajectories and the final geometries for non-uniform d_i in example 3 and 4 considered in subsection 5.1.4.3.2.	220
5.8	Multistatic TOA configuration with one transmitter and three receivers. The blue triangle represents the target, the green circle is the transmitter, and the red circles denote the receivers. θ_1, θ_2 and θ_3 are the azimuthal angles of the receivers and θ_0 is the azimuthal angle of transmitter, measured anticlockwise from the positive x-axis. $\mathbf{u}_1, \mathbf{u}_2$ and \mathbf{u}_3 are the unit vectors on the line connecting the receivers and the target, and \mathbf{u}_0 is the unit vector on the line connecting the transmitter to the target.	230
5.9	Convergence plot and corresponding receivers placement for 2D multistatic TOA configuration using D-optimal design. Uniform noise: (a) $M = 3, \sigma^2 = 1, \theta_1 = -60$ and $\theta_2 = \theta_3 = 60$; (b) $M = 4, \sigma^2 = 1, \theta_1 = \theta_4 = -60$ and $\theta_2 = \theta_3 = 60$. Nonuniform noise: (c) $M = 3, \mathbf{R} = \text{diag}(0.61, 0.82, 0.89), \theta_1 = 60$ and $\theta_2 = \theta_3 = -60$. (d) $M = 4, \mathbf{R} = \text{diag}(0.10, 0.15, 0.63, 0.86), \theta_1 = 60$ and $\theta_2 = \theta_3 = \theta_4 = -60$	242
5.10	Convergence plot and corresponding receivers placement for 3D multistatic TOA configuration using D-optimal design. Uniform noise ($\sigma^2 = 1$): (a) $M = 4, \boldsymbol{\theta} = [81.99, -98.01, -8.01, 171.99]^T$ and $\{\phi\}_{i=1}^4 = 70.53$; (b) $M = 5, \boldsymbol{\theta} = [-12.60, 59.40, 131.40, -156.60, -84.60]^T$ and $\{\phi\}_{i=1}^5 = 70.53$. Nonuniform noise (c) $\mathbf{R} = \text{diag}(0.90, 0.09, 0.32, 0.89), M = 4, \boldsymbol{\theta} = [-124.83, -4.83, 115.17, -124.83]^T$ and $\{\phi\}_{i=1}^4 = 70.53$; (d) $M = 5, \mathbf{R} = \text{diag}(0.42, 0.53, 0.93, 0.90, 0.54), \{\phi\}_{i=1}^5 = 70.53$, and $\boldsymbol{\theta} = [35.60, 168.90, 120.56, -50.63, -97.79]^T$	243
5.11	Convergence plot and corresponding receivers placement for 2D multistatic TOA configuration using A-optimal design. Uniform noise: (a) $M = 3, \sigma^2 = 1, \theta_1 = \theta_2 = -82.05$ and $\theta_3 = 59.77$; (b) $M = 4, \sigma^2 = 1, \theta_1 = \theta_2 = 70.53$ and $\theta_3 = \theta_4 = -70.53$; Nonuniform noise: (c) $M = 3, \mathbf{R} = \text{diag}(0.16, 0.79, 0.31), \theta_1 = \theta_2 = -65.38$ and $\theta_3 = 75.89$; (d) $M = 4, \mathbf{R} = \text{diag}(0.12, 0.10, 0.11, 0.65), \theta_1 = \theta_3 = 77.32$ and $\theta_2 = \theta_4 = -64.00$	244

- 5.12 Convergence plot and corresponding receivers' placement for **3D** multistatic TOA configuration using **A-optimal** design. **Uniform** noise: (a) $M = 4$, $\sigma^2 = 1$, $\boldsymbol{\theta} = [-61.63, 68.37, 151.63, -118.36]^T$ and $\{\phi\}_{i=1}^4 = 81.10$; (b) $M = 5$, $\sigma^2 = 1$, $\boldsymbol{\theta} = [33.44, 105.44, 177.44, -110.55, -38.55]^T$ and $\{\phi\}_{i=1}^5 = 81.10$. **Nonuniform** noise: (c) $M = 4$, $\{\phi\}_{i=1}^4 = 81.10$, $\mathbf{R} = \text{diag}(0.78, 0.82, 0.74, 0.79)$, $\boldsymbol{\theta} = [16.14, -71.30, 109.69, -157.64]^T$; (d) $M = 5$, $\mathbf{R} = \text{diag}(0.23, 0.44, 0.92, 0.32, 0.28)$, $\{\phi\}_{i=1}^5 = 81.10$. and $\boldsymbol{\theta} = [61.24, -105.76, -175.12, 165.20, -41.13]^T$ 245
- 5.13 Average computation time versus number of sensors for (a) 2D case and (b) 3D case. 248
- 5.14 A pictorial illustration of the multi-modal nature of the objective function: a 2-D contour plot of the objective function with respect to θ_3 and θ_4 , where θ_1 and θ_2 are fixed at their optimal values for $M = 4$ sensors for (a) D -optimal design and (b) A -optimal design. 248
- 5.15 The transmitter is also a receiver: Convergence plot and corresponding receivers placement for **2D** multistatic TOA configuration using **D-optimal** design. **Uniform** noise variances: (a) $M = 5$, $\sigma^2 = 1$, $\theta_1 = \theta_3 = 63.38$ and $\theta_2 = \theta_4 = \theta_5 = -67.57$. (b) $M = 6$, $\sigma^2 = 1$, and $\theta_1 = \theta_4 = \theta_5 = -64.54$ and $\theta_2 = \theta_3 = \theta_6 = 64.54$. **Non-uniform** noise variances: (c) $M = 5$, $\mathbf{R} = \text{diag}(1, 0.40, 0.72, 0.42, 0.99, 0.54)$, $\theta_1 = \theta_5 = -62.70$ and $\theta_2 = \theta_3 = \theta_4 = 63.44$. (d) $M = 6$, $\mathbf{R} = \text{diag}(1, 0.91, 0.23, 0.69, 0.64, 0.16, 0.29)$, $\theta_1 = \theta_3 = \theta_5 = -61.49$ and $\theta_2 = \theta_4 = \theta_6 = 61.67$. (The first element in \mathbf{R} is the noise variance at the transceiver) 250
- 5.16 The transmitter is also a receiver: Convergence plot and corresponding receivers placement for **3D** multistatic TOA configuration using **D-optimal** design. **Uniform** noise variances ($\sigma^2 = 1$): (a) $M = 4$, $\boldsymbol{\theta} = [-52.80, 37.17, 127.10, -142.87]^T$ and $\{\phi\}_{i=1}^4 = 76.61$; (b) $M = 5$, $\boldsymbol{\theta} = [-149.85, -5.65, 138.07, -77.69, 66.18]^T$ and $\{\phi\}_{i=1}^5 = 75.62$; . **Non-uniform** noise variances: (c) $M = 4$, $\mathbf{R} = \text{diag}(1, 0.70, 0.58, 0.58, 0.54)$, $\boldsymbol{\theta} = [162.82, 79.88, -114.88, -17.69]^T$ and $\{\phi\}_{i=1}^4 = 74.50$. (d) $M = 5$, $\mathbf{R} = \text{diag}(1, 0.72, 0.95, 0.52, 0.70, 0.59)$, $\boldsymbol{\theta} = [-89.09, 146.96, -9.91, -153.84, 81.45]^T$ and $\{\phi\}_{i=1}^4 = 74.10$. (The first element in \mathbf{R} is the noise variance at the transceiver) 251

- 5.17 The transmitter is also a receiver: Convergence plot and corresponding sensor placement for **2D** multistatic TOA configuration using **A-optimal** design. **Uniform** noise variances: (a) $M = 5$, $\sigma^2 = 1$, $\theta_1 = \theta_3 = \theta_5 = 83.25$ and $\theta_2 = \theta_4 = -72.24$. (b) $M = 6$, $\sigma^2 = 1$, $\theta_1 = \theta_3 = \theta_6 = 76.62$ and $\theta_2 = \theta_4 = \theta_5 = -76.62$. **Non-uniform** noise variances: (c) $M = 5$, $\mathbf{R} = \text{diag}(0.51, 0.98, 0.90, 0.65, 0.98, 0.16)$, $\theta_1 = \theta_2 = \theta_3 = \theta_4 = 63.52$ and $\theta_5 = -80.79$. (d) $M = 6$, $\mathbf{R} = \text{diag}(0.80, 0.16, 0.14, 0.90, 0.35, 0.16, 0.87)$, $\theta_1 = \theta_5 = -73.18$ and $\theta_2 = \theta_3 = \theta_4 = \theta_6 = 71.83$. (The first element in \mathbf{R} is the noise variance at the transceiver) 252
- 5.18 The transmitter is also a receiver: Convergence plot and corresponding receivers placement for **multistatic** TOA configuration using **A-optimal** design. **Uniform** noise variances: (a) $M = 4$, $\sigma^2 = 1$, $\boldsymbol{\theta} = [88.84, -0.98, 179.02, -90.81]^T$ and $\{\phi\}_{i=1}^4 = 86.70$; (b) $M = 5$, $\sigma^2 = 1$, $\boldsymbol{\theta} = [-158.65, -14.64, -86.76, 57.55, 129.53]^T$ and $\{\phi\}_{i=1}^5 = 85.98$; **Non-uniform** noise variances: (c) $M = 4$, $\mathbf{R} = \text{diag}(1, 0.27, 0.25, 0.80, 0.24)$, $\boldsymbol{\theta} = [43.99, 178.00, 99.85, -67.38]^T$ and $\{\phi\}_{i=1}^4 = 83.50$. (d) $M = 5$, $\mathbf{R} = \text{diag}(1, 0.71, 0.52, 0.91, 0.39, 0.60)$, $\{\phi\}_{i=1}^4 = 84.42$ and $\boldsymbol{\theta} = [-88.29, -45.61, 23.62, 115.53, -8.93]^T$. (The first element in \mathbf{R} is the noise variance at the transceiver) 253
- 5.19 A pictorial representation of the sensing scenario with $m = 5$ independent transmit/receive units: \mathcal{A} denotes the actual surveillance region while $\mathcal{R}_1 - \mathcal{R}_5$ represent the feasible deployment regions. 265
- 5.20 Objective of Problem \mathcal{P}_1^{TOA} versus iteration index. 280
- 5.21 Optimized sensor positions obtained by solving (a) \mathcal{P}_2^{TOA} , (b) \mathcal{P}_4^{TOA} and (c) \mathcal{P}_3^{RSS} with constraint that the i^{th} sensor lies inside the regions \mathcal{R}_i . ‘ \cdot ’ markers are the grid points in the source region and red stars are the sensor positions obtained via the developed algorithms. 282
- 5.22 Optimized sensor positions obtained by solving (a) \mathcal{P}_1^{TOA} , (b) \mathcal{P}_3^{TOA} and (c) \mathcal{P}_2^{RSS} with constraint that the i^{th} sensor lies inside the i^{th} ellipse (\mathcal{R}_i). ‘ \cdot ’ markers are the grid points in the source region and red stars are the sensor positions. 285
- 5.23 Optimized sensor positions obtained by solving (a) \mathcal{P}_1^{TOA} , (b) \mathcal{P}_1^{RSS} and (c) \mathcal{P}_4^{RSS} with constraint that the sensors lie in the annular region \mathcal{R} . ‘ \cdot ’ markers are the grid points in the source region and red stars are the sensor positions. 286
- 5.24 Optimized sensor positions obtained by solving (a) \mathcal{P}_1^{TOA} and (b) \mathcal{P}_1^{RSS} with constraint that the i^{th} sensor lies inside \mathcal{R}_i . Red circles are the sensor positions obtained via our developed algorithm. 288
- 5.25 Optimized sensor positions obtained by solving (a) \mathcal{P}_3^{TOA} and (b) \mathcal{P}_3^{RSS} with constraint that the sensors lie in and annular region \mathcal{R} . Red circles are the sensor positions obtained via our algorithm. 289

List of Tables

3.1	Average number of iterations needed by each algorithm for synthetic data	42
3.2	Average number of iterations needed by each algorithm for real data .	43
3.3	Confusion matrix in the context of graph learning	66
3.4	Performance measures of the competing methods for MRI data	70
3.5	Performance measures of the competing methods for migration data .	72
3.6	Performance measures of the competing methods for ionosphere data	73
3.7	Confusion matrix in the context of hypothesis testing	110
3.8	Comparison of the average time taken by the BCD and the PD algorithms	113
5.1	Comparison between previous hybrid sensor placement studies and the proposed algorithm	190
5.2	Computation complexity of the proposed algorithm for A –, D – and E –optimal designs	212
5.3	Comparison of theoretical and numerical value of trace of CRLB . . .	217
5.4	Angles (in degrees) of the optimal sensor-target geometries obtained .	220
5.5	Comparison of the MLE performance for different placement	222
5.6	Comparison of the MLE performance of sensor placement for target localization mismatch	223
5.7	Comparison of the proposed method with state-of-the-art methods . .	228
5.8	Comparison of the objective function values obtained using A –optimal and D –optimal designs for 2D scenario analyzed in Section 5.2.4.1 .	246
5.9	Comparison of the objective function values obtained using A –optimal and D –optimal designs for 3D scenario analyzed in Section 5.2.4.1 .	247
5.10	Comparison of the objective function values obtained using A –optimal and D –optimal designs for 2D scenario analyzed in Section 5.2.4.2 .	254
5.11	Comparison of the objective function values obtained using A –optimal and D –optimal designs for 3D scenario analyzed in Section 5.2.4.2 .	254
5.12	Target localization performance for the proposed method	256
5.13	Comparison between related previous studies and this paper.	259
5.14	Comparison of the design objectives obtained using different placements for the 2D configurations analyzed in Subsection 5.3.4.1	284

5.15	Comparison of the design objectives obtained using different placements for the 2D configurations analyzed in Subsection 5.3.4.1	286
5.16	Comparison of the design objectives obtained using different placements for the 2D configurations analyzed in Subsection 5.3.4.1	287
5.17	Comparison of the design objectives obtained using different placements for the 3D configurations analyzed in Subsection 5.3.4.2	288
5.18	Comparison of the design objectives obtained using different placements for the 3D configurations analyzed in Subsection 5.3.4.2	289
5.19	Comparison of the MLE performance for different placement assuming TOA based localization.	291

Abbreviations

2D	2-Dimensional
3D	3-Dimensional
ADMM	Alternating Direction Method of Multipliers
AOA	Angle Of Arrival
BCD	Block Coordinate Descent
BN	Bayesian Network
CGL	Cobinatorial Graph Laplacian
CRB	Cramer-Rao Bound
CRLB	Cramer-Rao Lower Bound
DFT	Discrete Fourier Transform
EBIC	Extended Bayesian Information Criterion
ER	Erdos Renyi
FDR	False Discovery Rate
FIM	Fisher Information Matrix
GGM	Gaussian Graphical Model
GL	Graph Learning
GLASSO	Graphical LASSO
GMRF	Gaussian Markov Random Field
GSP	Graph Signal Processing
KKT	Karush-Kuhn-Tucker
KL	Kullback Liebler
LOS	Line of Sight
LS	Least Squares
MCC	Matthews Correlation Coefficient
ML	Maximum Likelihood
MLE	Maximum Likelihood Estimation

MM	M ajorization- M inimization
MRF	M arkov R andom F ield
MM	M ajorization- M inimization
MSE	M ean S quared E rror
NRMSE	N ormalized R oot M ean S quare E rror
PD	P roximal D istance
PDMM	P rimal- D ual M ajorization- M inimization
PG	P oisson plus G aussian
PGM	P robabilistic G raphical M odel
PGPAL	P oisson- G aussian P hase-retrieval A lgorithm
PR	P hase- R etrieval D ifference
PSD	P ositive S emi- D efinite
RMSE	R oot M ean S quare E rror
RSS	R eceived S ignal S trength
SCM	S ample C ovariance M atrix
SDP	S emidefinite P rogramming
SNR	S ignal to N oise R atio
SOCP	S econd O rders C one P rogramming
TDOA	T ime D ifference O f A rrival
TOA	T ime O f A rrival
TSOA	T ime S um of A rrival
TV	T otal V ariation
WF	W irtinger F low
WLS	W eighted L east S quares

Notations

x	Scalar
\mathbf{x}	Vector
\mathbf{X}	Matrix
x_i	i^{th} element of vector \mathbf{x}
$X_{i,j}$	$(i, j)^{\text{th}}$ element of the matrix \mathbf{X}
\mathbf{x}_i	i^{th} column of the matrix \mathbf{X}
$\mathbb{R}^{m \times 1}$	Set of m dimensional vectors of real numbers
$\mathbb{R}^{m \times m}$	Set of $m \times m$ matrices of real numbers
\mathbb{N}	set of natural numbers
\ln	natural logarithm
\log	logarithm with base 10
$\tan^{-1}(x)$	arctangent value of x
$\cos^{-1}(x)$	arccosine value of x
$\sin^{-1}(x)$	arcsine value of x
$(\cdot)^T$	Transpose
$(\cdot)^{-1}$	Inverse
\otimes	Kronecker product
$ \mathbf{X} $ or $\det(\mathbf{X})$	Determinant of matrix \mathbf{X}
$\text{Tr}(\mathbf{X})$	Trace of matrix \mathbf{X}
\mathbf{X}^2	Square of matrix \mathbf{X}
\mathbf{I}_N	Identity matrix of size N
$\text{diag}(\mathbf{x})$	a diagonal matrix with diagonal values from vector \mathbf{x}
∇f	Gradient of a function f
$\nabla^2 f$	Hessian of a function f .
$\frac{\partial(\cdot)}{\partial x}$	first-order derivative with respect to x
$\frac{\partial^2(\cdot)}{\partial x^2}$	second-order derivative with respect to x

$\mathbf{X} \succeq 0$	\mathbf{X} is a PSD matrix
$\mathbf{X} \succeq \mathbf{Y}$	matrix $\mathbf{X} - \mathbf{Y}$ is symmetric positive semi-definite
$\mathbf{X} \succ 0$	\mathbf{X} is a positive definite matrix
$\lambda(\mathbf{X})$	Maximum eigenvalue of matrix \mathbf{X}
$\ \mathbf{x}\ $	Euclidean norm of the vector \mathbf{x}
$\ \mathbf{x}\ _1$	ℓ_1 norm of the vector \mathbf{x}
$\ \mathbf{X}\ _F$	Frobenious norm of matrix \mathbf{X}
$\mathbf{E}(\cdot)$	Statistical expectation
\circ	Element wise multiplication.
$\text{sgn}(\cdot)$	signum (or sign) function
$p(\mathbf{x})$	probability density function of the random variable \mathbf{x}
$x \sim \mathcal{N}(\mu, \sigma^2)$	x is Gaussian random variable with a mean of μ and variance of σ^2
$\mathcal{U}(x, y)$	uniform distribution taking values between x and y
$\mathbf{x} \in \mathcal{X}$	\mathbf{x} is element of the set \mathcal{X}
$\mathbf{x}^k/\mathbf{x}^t, \mathbf{X}_k/\mathbf{X}_t$	values of the vector \mathbf{x} and matrix \mathbf{X} at the $k^{\text{th}}/t^{\text{th}}$ iteration, respectively